Available online at www.sciencedirect.com
SCIENCE DIRECT®
Nuclear Instruments and Methods in Physics Research B 249 (2006) 29–33
NIM B
Beam Interactions with Materials & Atoms
www.elsevier.com/locate/nimb

Electronic energy loss of swift H^+ and He^+ ions in solids with material science applications

Juan Carlos Moreno-Marín [a], Isabel Abril [b], Santiago Heredia-Avalos [c,*], Rafael Garcia-Molina [c]

[a] Departamento de Física, Enginyeria de Sistemes i Teoria del Senyal, Universitat d'Alacant, Apartat 99, E-03080 Alacant, Spain
[b] Departamento de Física Aplicada, Universitat d'Alacant, Apartat 99, E-03080 Alacant, Spain
[c] Departamento de Física, Universidad de Murcia, Apartado 4021, E-30080 Murcia, Spain

Available online 6 May 2006

Abstract

We calculate the electronic energy loss of swift H^+ and He^+ ion beams in several solids with applications in material science and microelectronics, namely Ti, Fe, Ge, Pd, LiF and Si_3N_4. Our calculations are based on the dielectric formalism, where the charge density of the projectile is described by the Brandt–Kitagawa model, with the addition of projectile polarization. We take into account the different charge states of the projectile inside the target and the energy loss due to electron capture and loss processes. Using a realistic description of the target energy loss function, we obtain results that show a good agreement with available experimental data in a wide range of projectile energies.

PACS: 34.50.Bw; 77.22.−d; 47.27.Vf; 61.46.+w

Keywords: Energy loss of light ions; Electronic stopping power; Dielectric properties of solids; Energy loss function

1. Introduction

A precise knowledge of the energy loss of swift ions in solids is necessary in the materials science and microelectronics industry, for both target properties modification and structural characterization by ion beam methods [1]. The scarce or absence of experimental data for ion energy loss in materials of technological interest, specially compound materials, makes it desirable to have reasonably accurate theoretical predictions.

In this work we theoretically evaluate the electronic energy loss of swift H^+ and He^+ in solids with applications in materials science and microelectronics; we consider both elemental targets (Ti, Fe, Ge and Pd) and compound materials (LiF and Si_3N_4) [2–4]. We use the dielectric formalism framework with a realistic description of both the target and the projectile [5–9], taking into account the projectile polarization, the different charge state the projectile can acquire during its travel through the target, as well as the energy loss associated to the electron capture and loss processes. For the projectile energies we consider in this work, the nuclear energy loss is negligible.

This paper is organized as follows. The theoretical model is described in Section 2, whereas our results are presented and compared with the experimental data in Section 3. Finally the conclusions are given in Section 4.

2. Model description

When a projectile, with atomic number Z_1 and charge state q, impinges with velocity v on a solid, its charge state changes due to electron capture and loss processes. Therefore in the dynamical equilibrium between all the possible projectile charge states, the total electronic stopping power $S_p(v)$ of the solid will be a weighted sum of the stopping

* Corresponding author. Tel.: +34 968 367383; fax: +34 968 36 41 48.
E-mail address: sheredia@um.es (S. Heredia-Avalos).

0168-583X/$ - see front matter © 2006 Elsevier B.V. All rights reserved.
doi:10.1016/j.nimb.2006.03.016

power due to each charge state of the projectile, $S_{\mathrm{p},q}(v)$, plus the stopping power due to electronic capture and loss processes, $S^{\mathrm{CL}}_{\mathrm{p},q}(v)$, that is,

$$S_{\mathrm{p}}(v) = \sum_{q=0}^{Z_1} \phi_q S_{\mathrm{p},q}(v) + S^{\mathrm{CL}}_{\mathrm{p},q}(v), \tag{1}$$

where the sum is extended over all the possible charge states of the projectile. The CasP 3.1 code [10] is used to evaluate the fraction ϕ_q of the q charge state at equilibrium, which depends on the target, the projectile and its velocity. We have extended the model proposed in [11] to estimate $S^{\mathrm{CL}}_{\mathrm{p},q}(v)$.

The stopping power of the target, $S_{\mathrm{p},q}(v)$, for a projectile with a charge state q is evaluated using the dielectric formalism, including the contribution of the projectile polarization (due to the electric field induced by the projectile in the target). This self-induced electric field displaces a distance d_q the center of the projectile electronic cloud from its nucleus. Then we write [11]

$$\begin{aligned} S_{\mathrm{p},q}(v) = {} & \frac{2Z_1^2e^2}{\pi v^2}\int_0^\infty \frac{\mathrm{d}k}{k}\int_0^{kv}\mathrm{d}\omega\ \omega \mathrm{Im}\left[\frac{-1}{\epsilon(k,\omega)}\right] \\ & + \frac{2e^2}{\pi v^2}\int_0^\infty \frac{\mathrm{d}k}{k}\rho_q^2(k)\int_0^{kv}\mathrm{d}\omega\ \omega \mathrm{Im}\left[\frac{-1}{\epsilon(k,\omega)}\right] - \frac{4Z_1e^2}{\pi v^2} \\ & \times \int_0^\infty \frac{\mathrm{d}k}{k}\rho_q(k)\int_0^{kv}\mathrm{d}\omega\ \omega \mathrm{Im}\left[\frac{-1}{\epsilon(k,\omega)}\right]\cos\left(\frac{\omega \mathrm{d}_q}{v}\right), \end{aligned} \tag{2}$$

where $\hbar k$ and $\hbar\omega$ are, respectively, the momentum and energy transferred to electronic excitations of the target, $\rho_q(k)$ is the Fourier transform of the projectile electronic density for the q charge state, and $\mathrm{Im}[-1/\epsilon(k,\omega)]$ is the target energy loss function (ELF), which characterizes its response to external perturbations.

The first and second terms in Eq. (2) correspond to the stopping power for the projectile nucleus and its electronic cloud, respectively, whereas the third term accounts for interference effects [11]. The distance d_q is obtained as $d_q = \alpha_q \mathscr{E}_q(v)/e$, with α_q and $\mathscr{E}_q(v)$ being, respectively, the projectile polarizability and the self-induced electric field produced by the projectile,

$$\begin{aligned} \mathscr{E}_q(v) = {} & \frac{2e}{\pi v^2}\int_0^\infty \frac{\mathrm{d}k}{k}[Z_1 - \rho_q(k)] \\ & \times \int_0^{kv}\mathrm{d}\omega\ \omega\ \mathrm{Im}\left[\frac{-1}{\epsilon(k,\omega)}\right]. \end{aligned} \tag{3}$$

The charge density of the projectile is described by the Brandt–Kitagawa statistical model [12] considering the modification proposed in [13] for K-shell electrons. The electronic excitations of the target are separated in two contributions: those due to the outer electrons (modelled by a sum of Mermin-type energy loss function) and those of the inner-shell electrons (described by generalized oscillator strengths (GOS)) [8].

The interaction between the projectile and the outer electrons of the target is complicated due to the effect of chemical bonding and the existence of collective excitations. We build the ELF for these electrons by a fit to the experimental ELF in the optical limit (momentum transfer $\hbar k = 0$) for a wide range of transferred energies,

$$\begin{aligned} \mathrm{Im}\left[\frac{-1}{\epsilon(k=0,\omega)}\right]_{\mathrm{outer}} &= \sum_i A_i \mathrm{Im}\left[\frac{-1}{\epsilon_{\mathrm{M}}(k=0,\omega;\omega_i,\gamma_i)}\right]_{\omega \geqslant \omega_{\mathrm{th},i}} \\ &= \mathrm{Im}\left[\frac{-1}{\epsilon(k=0,\omega)}\right]_{\mathrm{exp}}, \end{aligned} \tag{4}$$

where ϵ_{M} is a Mermin-type ELF [14], and the fitting parameters ω_i, γ_i and A_i are related, respectively, with the position, the width and the intensity of the peaks and other structures observed in the ELF; $\hbar\omega_{\mathrm{th},i}$ is a threshold energy in this fitting procedure. Proceeding in this manner the chemical effects are included in the calculated stopping power of compound targets [15].

On the other hand, the excitations of the inner-shell electrons are described in terms of the GOS for isolated atoms; this approach is suitable because these electrons have large binding energies and show negligible collective effects. In this scheme, the electronic inner-shell contribution to ELF of a compound $\mathrm{A}_{\beta_1}\mathrm{B}_{\beta_2}\ldots$ can be obtained as

$$\mathrm{Im}\left[\frac{-1}{\epsilon(k,\omega)}\right]_{\mathrm{inner}} = \frac{2\pi^2\mathscr{N}}{\omega}\sum_j \beta_j \sum_{n,\ell}\frac{\mathrm{d}f^{(j)}_{n\ell}(k,\omega)}{\mathrm{d}\omega}, \tag{5}$$

where $\mathrm{d}f^{(j)}_{n\ell}(k,\omega)/\mathrm{d}\omega$ is the GOS for the (n,ℓ) subshell of the jth element and $\mathscr{N}$ is the molecular density of the target compound. The sums extend over all the inner subshells of the atoms in the compound. We assume that a given subshell can only be excited if the energy transferred to the target atom is larger than its ionization energy. We use the hydrogenic approach for the GOS because it is analytical and gives realistic values of the K- and L-shell ionization cross-sections [1,16].

When no experimental optical ELF at large values of $\hbar\omega$ is available for a compound $\mathrm{A}_{\beta_1}\mathrm{B}_{\beta_2}\ldots$, the ELF calculated with Eq. (5) is checked against the ELF given by

$$\mathrm{ELF} = \mathscr{N}\sum_j \beta_j \frac{\mathrm{ELF}_j}{n_j} \tag{6}$$

which results from the additivity of the ratios ELF_j/n_j, where n_j and ELF_j are, respectively, the atomic density and the ELF of each atomic constituent. The latter being obtained from the experimental X-ray scattering factors [17]. Although the results coming from Eq. (6) are not be reliable for energies corresponding to the excitation of the outer electrons, they are right for energies comparable to those of the inner-shells, because these internal electrons remain practically insensitive to the formation of the compound.

We have checked that the whole ELF we have modelled at $\hbar k = 0$ verifies the f-sum rule for the effective number of electrons in the target; this is also satisfied for all values of $\hbar k$ due to the analytical properties of the Mermin-type ELF. As an additional checking, we calculate the mean

excitation energy, I, of the target obtaining: $I(\mathrm{Ti}) = 238$ eV, $I(\mathrm{Fe}) = 280$ eV, $I(\mathrm{Ge}) = 368.6$ eV, $I(\mathrm{Pd}) = 450.5$ eV, $I(\mathrm{LiF}) = 86.4$ eV and $I(\mathrm{Si_3N_4}) = 140$ eV, in good agreement with available experimental data [18].

3. Results and discussions

We show in Fig. 1 the ELF at $\hbar k = 0$ of Ti, Fe, Ge, Pd, LiF and Si_3N_4, as a function of the excitation energy. For each target, the solid line corresponds to our fitting based on Eqs. (4) and (5), the left side of the figure is due to excitations of the most outer electrons, whereas the right side, in a logarithm scale, is due to the excitations of the inner-shell electrons. The parameters used to fit the contribution of the outer electrons to the ELF, Eq. (4), appear in Table 1. The experimental data of the ELF for each target are represented by symbols [19]. For higher energies, where experimental data are not available to compare with, the ELF of the compound is calculated according to Eq. (6). The GOSs we have used to describe the excitations of the inner-shell electrons clearly appear as sharp edges in the ELF for high transferred energies, namely the excitations of the K-shell electrons for F, Si and N, and the excitations of the K- and L-shell electrons for Ti, Fe, Ge and Pd.

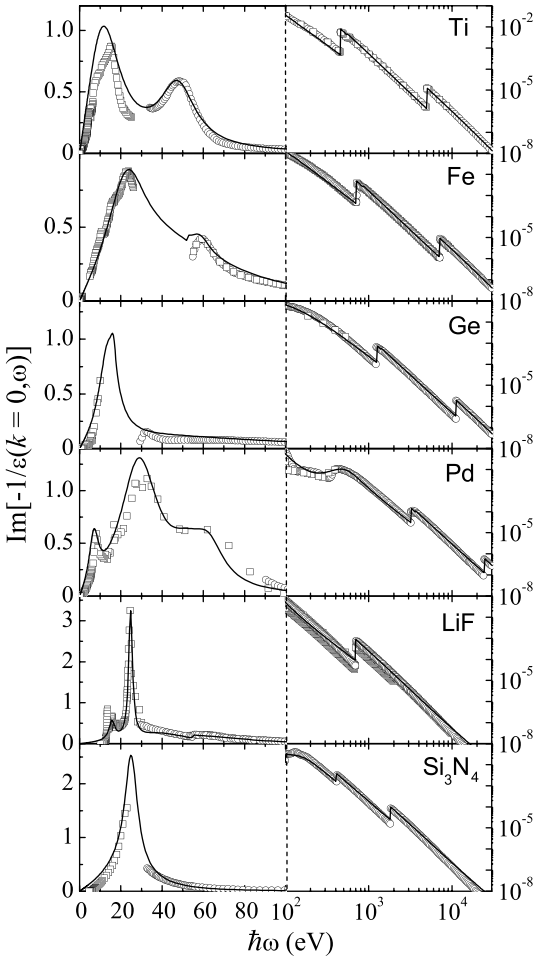

Fig. 1. Energy loss function (ELF) in the optical limit, $\hbar k = 0$, of Ti, Fe, Ge, Pd, LiF and Si_3N_4, as a function of the excitation energy. The solid line represents our fitting to the experimental ELF, denoted by □ [19], and to the reconstructed ELF from the X-ray scattering factors, represented by ○ [17].

Table 1
Parameters used to fit the optical ELF corresponding to the outer electrons of Ti, Fe, Ge, Pd, LiF and Si_3N_4

Target [D (g/cm^3)]	i	$\hbar\omega_{\mathrm{th},i}$ (eV)	$\hbar\omega_i$ (eV)	$\hbar\gamma_i$ (eV)	A_i
Ti [4.5]	1		15.0	21.0	1.19
	2		47.6	122.4	1.04×10^{-1}
	3		48.4	21.22	2.18×10^{-1}
Fe [7.86]	1		25.3	22.6	5.09×10^{-1}
	2		55.8	87.1	5.00×10^{-1}
	3	52.8	58.5	10.3	1.73×10^{-2}
Ge [5.32]	1		14.8	10.9	6.23×10^{-1}
	2		16.9	2.72	4.17×10^{-2}
	3		83.0	190.5	1.81×10^{-1}
Pd [12.02]	1		7.3	5.4	3.43×10^{-1}
	2		30.7	22.6	8.85×10^{-1}
	3		52.5	21.8	1.07×10^{-1}
	4		62.9	18.5	1.07×10^{-1}
	5		512.0	435.0	8.21×10^{-3}
LiF [2.635]	1		15.6	3.5	1.03×10^{-1}
	2		24.6	2.3	2.87×10^{-1}
	3		42.9	36.7	2.02×10^{-1}
	4	54.7	70.7	46.3	6.36×10^{-2}
Si_3N_4 [3.4]	1		25.1	7.35	6.09×10^{-1}
	2		25.3	26.9	4.86×10^{-1}
	3	99.8	152.4	163.3	2.23×10^{-2}

D is the atomic mass density of the target.

The stopping cross section (SCS) is a magnitude that is often used to quantify the energy loss per unit path length instead of the stopping power, because the former removes the dependence on the target density. It is defined as $\mathrm{SCS} = S_p M_2/D$, where M_2 and D are the atomic mass and the density of the target, respectively. In Fig. 2 we show the SCSs of Ti, Fe, Ge, Pd, LiF and Si_3N_4 for H^+ and He^+ projectiles, as a function of the energy per nucleon, using the previous representations of the target ELF and the projectile charge fractions from [10]. The solid curves correspond to the SCSs calculated using the modified Brandt–Kitagawa model [12,13] for $\rho_q(k)$, whereas the symbols represent experimental SCSs [4,21–25]. For comparison purposes, we have plotted as dashed curves the semi-empirical predictions of the SRIM-2003 code [20], which are based on fits to experimental stopping cross sections. It can be seen in Fig. 2 that the SCS calculations performed with the modified Brandt–Kitagawa model show a satisfactory agreement with most of the available experimental data, even at low projectile energies.

The polarization of the projectile increases the SCS for hydrogen projectiles by about 10–15% near the SCS maximum ($E \sim 30$ keV/nucleon), whereas we have checked that this phenomenon is negligible for helium projectiles

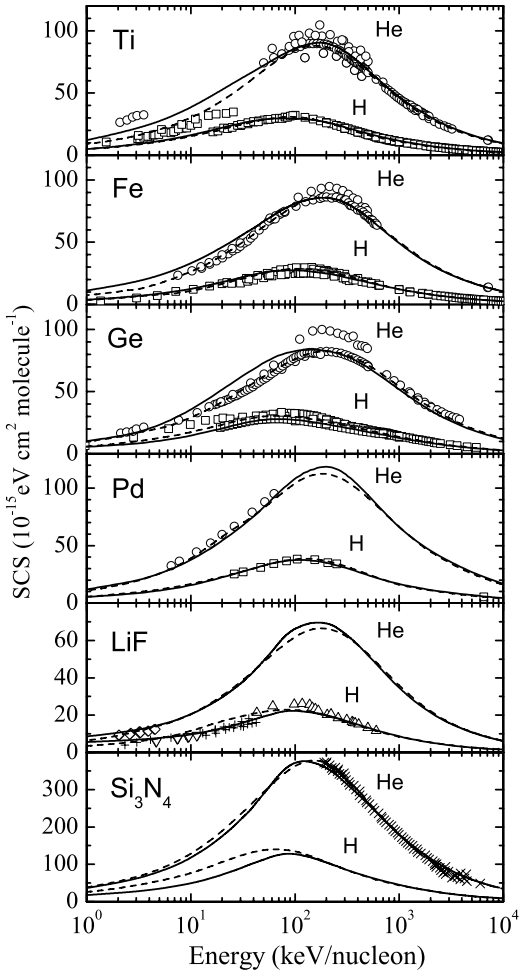

Fig. 2. Stopping cross section (SCS) of Ti, Fe, Ge, Pd, LiF and Si_3N_4, for H^+ and He^+ as a function of the projectile energy. Solid lines represent our calculations and dashed lines are SRIM-2003 predictions [20]. Symbols refer to experimental data: H^+ (□) and He^+ (○) in Ti, Fe, Ge and Pd [21]; H^+ in LiF (△ [22], ▽ [23], + [24]), He^+ in LiF (◇ [25]) and in Si_3N_4 (× [4]).

because its low polarizability. All the same, such effect should be considered for other heavier projectiles with high polarizability, like lithium [11].

Our calculations take into account the chemical effect because the fitting of the low-energy region of the ELF to the experimental ELF of the compound target, where the major discrepancies from Bragg's additivity rule appear [15]. Obviously, the main contribution to the SCS is due to the outer electron excitations, however, when increasing the projectile energy the influence of the inner-shell electron excitations becomes more important. We find that the inner-shell electron excitations of the analyzed targets have a similar behavior; in particular, the L-shell contribution of Ti represents ~2% of the total SCS for a projectile energy of 300 keV/nucleon, whereas it is ~18% at 3000 keV/nucleon. In contrast, the K-shell contribution has no influence even at 3000 keV/nucleon, representing a contribution to the SCS less than 0.2%.

The contribution to the SCS due to electron capture and loss by the projectile represents ~5–15% of the total SCS near the SCS maximum for hydrogen projectiles and decreases as the projectile energy increases, being negligible for $\gtrsim 400$ keV/nucleon; this percentage drastically decreases for helium projectiles, being less than 3% near the SCS maximum. It is worth to mention that the contribution to the SCS due to electron capture and loss processes strongly increases as the projectile energy decreases, representing even ~25–60% of the total SCS for ~1 keV/nucleon.

4. Conclusion

In summary, we have employed the dielectric formalism to calculate the electronic stopping cross section of Ti, Fe, Ge, Pd, LiF and Si_3N_4 for swift H^+ and He^+ projectiles. Both the projectile charge density and the target ELF are properly described in this theoretical framework, the former through the modified BK model and the latter using a sum of Mermin-type ELF to describe the excitations of outer electrons and atomic GOSs to account for the excitation of inner-shell electrons. Then, the SCS was obtained as a weighted sum of all the contributions due to the different charge states that the swift ion can have inside the target plus the SCS due to the electron capture and loss processes. In addition, we consider in our calculations the polarization of the projectile due to the self-induced electric field.

The SCSs calculated through this procedure reproduce reasonably well the available experimental values in a wide range of projectile energies.

Acknowledgements

This work was supported by the Spanish Ministerio de Educación y Ciencia (Projects BFM2003-04457-C02-01 and BFM2003-04457-C02-02). S.H.A. thanks the Fundación Cajamurcia for a postdoctoral research grant.

References

[1] M.A. Kumakhov, F.F. Komarov, Energy Loss and Ion Ranges in Solids, Gordon and Breach, New York, 1981.
[2] A. Climent-Font, J. Räisänen, E. Rautala, Nucl. Instr. and Meth. B 136–138 (1998) 109.
[3] V. Mussi, R.M. Montereali, P. Moretti, J. Mugnier, E. Nichelatti, F. Osma, B. Jacquier, Nucl. Instr. and Meth. B 230 (2005) 257.
[4] C. Pascual-Izarra, Ph.D. Thesis, Universidad Autónoma de Madrid, 2004.
[5] I. Abril, R. Garcia-Molina, C. Denton, F.J. Pérez-Pérez, N.R. Arista, Phys. Rev. A 58 (1998) 357.
[6] J.C. Moreno-Marín, I. Abril, R. Garcia-Molina, Nucl. Instr. and Meth. B 193 (2002) 30.
[7] I. Abril, R. Garcia-Molina, N.R. Arista, C.F. Sanz-Navarro, Nucl. Instr. and Meth. B 190 (2002) 89.
[8] S. Heredia-Avalos, J.C. Moreno-Marín, I. Abril, R. Garcia-Molina, Nucl. Instr. and Meth. B 230 (2005) 118.
[9] S. Heredia-Avalos, R. Garcia-Molina, J.M. Fernández-Varea, I. Abril, Phys. Rev. A 72 (2005) 052902.
[10] P.L. Grande, G. Schiwietz, CasP. Convolution approximation for Swift Particles, version 3.1 (2005) code available at <http://www.hmi.de/people/schiwietz/casp.html>.

[11] S. Heredia-Avalos, R. Garcia-Molina, Nucl. Instr. and Meth. B 193 (2002) 15.
[12] W. Brandt, M. Kitagawa, Phys. Rev. B 25 (1982) 5631.
[13] W. Brandt, Nucl. Instr. and Meth. 194 (1982) 13.
[14] N.D. Mermin, Phys. Rev. B 1 (1970) 2362.
[15] P. Bauer, R. Golser, D. Semrad, P. Maier-Komor, F. Aumayr, A. Arnau, Nucl. Instr. and Meth. B 136–138 (1998) 103.
[16] R.F. Egerton, Electron Energy-Loss Spectroscopy in the Electron Microscope, Plenum Press, New York, 1989.
[17] B.L. Henke, E.M. Gullikson, J.C. Davis, At. Data Nucl. Data Tab. 54 (1993) 2. Available from: <http://xray.uu.se/hypertext/henke.html>.
[18] ICRU Report 49, Stopping Powers and Ranges for Protons and Alpha Particles, International Commission on Radiation Units and Measurements, Bethesda, 1993.
[19] E.D. Palik, G. Ghosh (Eds.), The Electronic Handbook of Optical Constants of Solids, Academic Press, San Diego, 1999.
[20] J.F. Ziegler, J.P. Biersak, SRIM. The Stopping and Range of Ions in Matter, Version (2003).20 Available from: <http://www.srim.org>.
[21] H. Paul, Experimental Stopping Power Compilation. Available from <http://www.exphys.uni-linz.ac.at/Stopping/>.
[22] M. Bader, R.E. Pixley, F.S. Moser, W. Whaling, Phys. Rev. 103 (1956) 32.
[23] K. Eder, D. Semrad, P. Bauer, R. Golser, P. Maier-Komor, F. Aumayr, M. Pealba, A. Arnau, J.M. Ugalde, P.M. Echenique, Phys. Rev. Lett. 79 (1997) 4112.
[24] S.P. Moller, A. Csete, T. Ichioka, H. Knudsen, U.I. Uggerhoj, H.H. Andersen, Phys. Rev. Lett. 93 (2004) 42502.
[25] J.I. Juaristi, C. Auth, H. Winter, A. Arnau, K. Eder, D. Semrad, F. Aumayr, P. Bauer, P.M. Echenique, Phys. Rev. Lett. 84 (2000) 2124.